Targeting Cellular Iron Homeostasis with Ironomycin in Diffuse Large B-cell Lymphoma

Julie Devin[1,2], Tatiana Cañeque[3], Yea-Lih Lin[2], Lucie Mondoulet[4], Jean-Luc Veyrune[2], Matthieu Abouladze[1,2], Elvira Garcia De Paco[1,2], Ouissem Karmous Gadacha[1,2], Guillaume Cartron[5], Philippe Pasero[2], Caroline Bret[1,6], Raphaël Rodriguez[3], and Jerome Moreaux[1,2,6,7]

ABSTRACT

Diffuse large B-cell lymphoma (DLBCL) is the most common hematological malignancy. Although more than half of patients with DLBCL achieve long-term remission, the majority of remaining patients succumb to the disease. As abnormal iron homeostasis is implicated in carcinogenesis and the progression of many tumors, we searched for alterations in iron metabolism in DLBCL that could be exploited to develop novel therapeutic strategies. Analysis of the iron metabolism gene expression profile of large cohorts of patients with DLBCL established the iron score (IS), a gene expression–based risk score enabling identification of patients with DLBCL with a poor outcome who might benefit from a suitable targeted therapy. In a panel of 16 DLBCL cell lines, ironomycin, a promising lysosomal iron-targeting small molecule, inhibited DLBCL cell proliferation at nanomolar concentrations compared with typical iron chelators. Ironomycin also induced significant cell growth inhibition, ferroptosis, and autophagy. Ironomycin treatment resulted in accumulation of DNA double-strand breaks, delayed progression of replication forks, and increased RPA2 phosphorylation, a marker of replication stress. Ironomycin significantly reduced the median number of viable primary DLBCL cells of patients without major toxicity for nontumor cells from the microenvironment and presented low toxicity in hematopoietic progenitors compared with conventional treatments. Significant synergistic effects were also observed by combining ironomycin with doxorubicin, BH3 mimetics, BTK inhibitors, or Syk inhibitors. Altogether, these data demonstrate that a subgroup of high-risk patients with DLBCL can be identified with the IS that can potentially benefit from targeting iron homeostasis.

Significance: Iron homeostasis represents a potential therapeutic target for high-risk patients with DLBCL that can be targeted with ironomycin to induce cell death and to sensitize tumor cells to conventional treatments.

Introduction

Diffuse large B-cell lymphoma (DLBCL) is the most common lymphoid malignancy in adults, accounting for up to 35% of non-Hodgkin lymphomas. DLBCL is characterized by its clinical and biological heterogeneity (1). Although DLBCL is curable in over 60% of patients with rituximab (R)-based chemotherapy regimens such as CHOP (cyclophosphamide, doxorubicin, vincristine and prednisone), the remainder develop recurrent or progressive disease that is often fatal (2). Therefore, novel therapeutic approaches are still needed to achieve an effective treatment for high-risk/refractory DLBCL.

Iron plays a central role in a large number of essential cellular functions (3), including oxygen sensing, energy metabolism, respiration and folate metabolism. Most importantly, iron is required for cell proliferation, serving as a cofactor for several enzymes involved in DNA synthesis and DNA repair (4). These proteins include the three DNA polymerases (Pol α, Pol δ and Pol ε) and primase, which require a Fe-S cluster for the formation of active holoenzymes. Moreover, the DNA helicases XPD FANCJ, ChlR1, and RTEL contain a conserved Fe-S cluster near the N-terminus, which is essential for their helicase activity (5). Moreover, the eukaryotic RNR small subunit (β or R2) requires iron to form a diferric-tyrosyl radical cofactor (Fe2-IIIY·) involved in the production of dNTPs (6). Given the essential role of iron in cell proliferation, rapidly growing tumor cells exhibit altered iron metabolism and elevated cellular iron uptake mediated by the transferrin receptor (TfR). Importantly, enhanced iron endocytosis and the central role of iron as rate limiting regulators of epithelial–mesenchymal plasticity has been reported (7).

The use of iron chelators as anticancer agents has been widely described in the literature. It has been shown that iron chelators exert their anticancer effect by altering the activity of biomolecules that are critical for the regulation of both cell cycle and apoptotic processes (8). Deferoxamine (DFO) and deferasirox (DFX) are clinically approved iron chelators used to treat iron overload in patients. These iron

[1]Department of Biological Hematology, CHU Montpellier, Montpellier, France. [2]Institute of Human Genetics, UMR 9002 CNRS-UM, Montpellier, France. [3]Chemical Biology of Cancer Laboratory, Institut Curie, 26 rue d'Ulm, 75248 Paris Cedex 05, France; PSL Université, Paris, France; CNRS UMR 3666, Paris, France; INSERM U1143, Paris, France. [4]SideRos, Paris, France. [5]Clinical Hematology, CHU Montpellier, Montpellier, France. [6]University of Montpellier, UFR Medicine, Montpellier, France. [7]Institut Universitaire de France (IUF), Paris, France.

Note: Supplementary data for this article are available at Cancer Research Online (http://cancerres.aacrjournals.org/).

Corresponding Authors: Jerome Moreaux, Department of Biological Hematology, Hôpital Saint-Eloi - CHRU de Montpellier, 80, av. Augustin Fliche, 34295 Montpellier Cedex 5, IGH - Institute of Human Genetics, CNRS UMR-UM 9002, Montpellier, France. Phone: 33-0-467337903; Fax: 33(0)467337036; E-mail: jerome.moreaux@igh.cnrs.fr; Raphaël Rodriguez, Chemical Biology of Cancer Laboratory, Institut Curie, 26 rue d'Ulm, 75248 Paris, France. Phone: 33-0-448482191; E-mail: raphael.rodriguez@curie.fr; and Caroline Bret, Department of Biological Hematology, Hôpital Saint-Eloi - CHRU de Montpellier, 80, av. Augustin Fliche, 34295 Montpellier Cedex 5, IGH - Institute of Human Genetics, CNRS UMR-UM 9002, Montpellier, France. Phone: 33-0-467337031; Fax: 33-0-467337036; E-mail: c-bret@chu-montpellier.fr

Cancer Res 2022;82:998–1012

doi: 10.1158/0008-5472.CAN-21-0218

chelators presented a potential interest to treat lymphoid malignancies like mantle cell lymphoma (9) or multiple myeloma (10). However, no iron chelators specifically developed for cancer treatment has been clinically approved.

Ironomycin is a synthetic derivative of salinomycin that presents an antineoplastic effect on breast cancer stem cells by accumulating and sequestering iron in lysosomes (11). Lysosomal iron mediates the production of reactive oxygen species (ROS) through Fenton chemistry leading to lysosomal membrane permeabilization and ferroptosis. In contrast to programmed cell death, ferroptosis is a vulnerability of cells characterized by the overwhelming, iron-dependent accumulation of lethal lipid ROS (12). Thus, ironomycin represents a promising therapeutic approach against other neoplasm.

In this study, we analyzed the iron metabolism gene expression profile (GEP) of large cohorts of patients with DLBCL to establish an "iron score" (IS), a GEP-based signature of key effectors of iron metabolism. This signature allowed the identification of a subgroup of patients with DLBCL with poor outcome that could benefit from an iron-targeted therapy. We also comparatively analyzed the effect of clinically approved iron chelators (deferoxamine and deferasirox) and ironomycin. Interestingly, ironomycin exhibited a significant toxicity against DLBCL cells at nanomolar concentrations compared with other iron chelators, illustrating distinct mechanisms of action. Ironomycin induced significant cell growth inhibition, ferroptosis and autophagy of DLBCL cells. We also observed an induction of replication stress with slower progression of replication forks, an increased phosphorylation of RPA2 and the accumulation of DNA double-strand breaks upon ironomycin treatment. Importantly, ironomycin significantly reduced the median number of viable primary DLBCL cells of patients without major toxicity for nontumor cells from the microenvironment. Furthermore, a significant synergistic effect was identified when ironomycin was combined with doxorubicin. Together, these data indicate that ironomycin represents an appealing therapeutic strategy in DLBCL and especially in high-risk patients defined by the IS.

Materials and Methods

Human DLBCL cell lines

The 16 DLBCL cell lines (U2932, OCI-LY-3, NU-DHL-1, OCI-LY-19, DB, SUDHL4, OCILY1, SUDHL5, DOHH2, SUDHL10, HT, RI-1, SU-DHL-6, NUDUL-1, WSU-DLCL-2 and OCI-LY-7) were purchased from the DSMZ (Leibniz-Institut DSMZ - Deutsche Sammlung von Mikroorganismen und Zellkulturen GmbH). They were maintained in RPMI-1640 (Gibco, Invitrogen), supplemented with 10% FBS (PAA laboratory GmbH) for U2932, SUDHL-4, HT, DOHH2, SUDHL-10, RI-1, WSU-DLCL-2 cell lines, 20% FBS OCI-LY3, DB, SUDHL-5, NUDHL-1, SU-DHL-6, NUDUL-1 cell lines. OCI-LY1 and OCI-LY7 were cultured in IMDM (Gibco, Invitrogen), supplemented with 20% FBS and OCI-LY19 was cultured in MEM alpha modified (Gibco, Invitrogen), supplemented with 20% FBS. Cell line identity was regularly checked by short-tandem repeat analysis, and cells were regularly screened for *Mycoplasma* contamination.

Reagents

Deferoxamine (Novartis Pharma SAS) was dissolved in sterile distilled water and deferasirox (Selleckchem S1712), was dissolved in dimethyl sulfoxide (DMSO) to a concentration of 300 and 50 mmol/L, respectively. Ironomycin was a kind gift of Raphaël Rodriguez team (11), this compound was dissolved in dimethyl sulfoxide (DMSO) to a concentration of 10 mmol/L. Other reagents: erastin (Selleckchem S7242, 10 mmol/L in DMSO), ferrostatin-1 (Selleckchem S7243, 50 mmol/L in DMSO), Q-VD Oph (SelleckChem S7311, 10 mmol/L in DMSO, 30′ pretreatment), iron(III) chloride hexahydrate (31232 Sigma Aldrich, 0.1 mol/L in water, 4 hours after treatment), reduced gluthatione GSH (Sigma Aldrich G4251, 0.1 M in PBS) H_2O_2 (Sigma Aldrich 216763), mafosfamide (surrogate of cyclophosphamide, Santa Cruz ChemCruz SC-211761, 10 mmol/L in saline water), gemcitabine (Sellekchem S1149, 50 mmol/L in saline water), doxorubicin (Sellekchem S1208, 20 mmol/L in DMSO), CldU (Abcam ab213715, 20 mmol/L), IdU (Abcam ab142581, 2 mmol/L), 3-methyl adenine (Merck, #189490), β-mercaptoethanol (Sigma, M3148), staurosporine (Selleckchem, S1421), ketokonazole (Sigma, UC280), Avasimibe (from Sigma, PZ0190), ibrutinib (from Sellekchem S2680), entospletinib (from Selleckchem, S7523), venetoclax (from Sellekchem, S8048), AZD-5991 (from Selleckchem, S8643), and A1155463 (from TargetMol, T6748).

Cell viability assay

DLBCL-derived cell lines were cultured for 4 days in 96-well flat-bottom microtiter plates in RPMI 1640 medium, 10% or 20% FCS (control medium) in the presence of various compounds. The number of viable cells in culture was determined using the CellTiter-Glo Luminescent Cell Viability Assay from Promega using a Centro LB 960 luminometer (Berthold Technologies).

This test is based on quantitation of the intracellular ATP present, which signals the presence of metabolically active cells. Data are expressed as the mean percentage of six replicates, normalized to the untreated control.

Flow cytometry analyses

The effects of deferoxamine, deferasirox or ironomycin on apoptosis, DNA damage and cell cycle after 24 and 72 hours of treatment were determined by flow cytometry using the Apoptosis, DNA Damage, and Cell Proliferation Kit (562253, Becton Dickinson) according to the manufacturer's instructions. Annexin V-PE staining for apoptosis analysis was performed using the "PE Annexin V Apoptosis Detection Kit I" (559763, Becton Dickinson). Flow cytometry analysis was done on a Fortessa flow cytometer (BD).

Hematopoietic progenitor colony-forming units assay

Mobilized peripheral blood cells from donor were collected after patients' written informed consent in accordance with the Declaration of Helsinki and Institutional Research Board approval from Montpellier University Hospital. CD34 cells from granulocyte colony stimulating factor–mobilized patients were purified using a MACS system (Miltenyi Biotec) according to the manufacturer's recommendations.

Two hundred and fifty viable $CD34^+$ cells/mL were cultured in Methocult GF H84434 Medium (Stem Cell, # 84434). Colonies were counted after 14 days of incubation at 37°C, with 5% CO_2 in a saturated humidified atmosphere.

Supplementary information concerning methodology is included in Supplementary experimental procedures.

Results

Considering the important role of iron homeostasis in cancer biology, we first aimed to identify iron metabolism genes associated with a prognostic value in DLBCL. A list of 62 genes involved in the regulation of iron homeostasis was identified from the literature (Supplementary Table S1; ref. 13). Analyzing this list of genes related to iron homeostasis using Maxstat R function and Benjamini

Hochberg multiple testing correction (14), 11 genes demonstrated a significant prognostic value in two independent cohorts of patients with DLBCL ($n = 233$ and $n = 181$, respectively; Supplementary Fig. S1A). High expression of three genes was associated with a good prognosis including *ALAS1* (Aminolevulinate, delta-synthase 1), *HIF1A* (hypoxia-inducible factor 1, alpha subunit), and *LRP2* (low density lipoprotein-related protein 2; Supplementary Fig. S1B). In contrast, high expression of eight other genes was associated with a poor prognosis. These include *HMOX1* [heme oxygenase (decycling) 1], *HMOX2* [heme oxygenase (decycling) 2], *HFE* (hemochromatosis), ISCA1 (iron-sulfur cluster assembly 1 homolog), *MSCP* (mitochondrial solute carrier protein), *PPOX* (protoporphyrinogen oxidase), *STEAP1* (six transmembrane epithelial antigen of the prostate 1), and *TMPRSS6* (transmembrane protease, serine 6; Supplementary Fig. S1C). We next combined the prognostic information of these genes in a GEP-based iron-score. The IS is defined by the sum of the beta coefficients of the Cox model for each prognostic gene, weighted by −1 according to the patient MMC signal above or below the probe set Maxstat value as previously described (14). Maxstat algorithm segregated the Lenz R-CHOP cohort into two groups with 39.5% of the patients with an IS > -0.168 and 60.5% of the patients with a IS ≤ -0.168 with a maximum difference in overall survival (OS; **Fig. 1A**). Patients with high-risk IS have a median OS of 50.6 months versus not reached for patients with low IS ($P = 3.7E-15$) in the Lenz R-CHOP cohort (**Fig. 1A**). The prognostic value of the IS was validated in the three additional independent cohorts for OS (**Fig. 1B–D**).

The IS is significantly higher in activated B-cell (ABC) DLBCL patients compared with germinal center B-cell (GCB) subgroup (**Fig. 1E**). Comparing the IS with other poor outcome-related factors, such as GCB/ABC subtype, age and the IPI in multivariate COX analysis, IS remained an independent prognostic factor (Supplementary Table S1). GSEA analysis revealed that IS defining high-risk patients are associated with a significant enrichment in MYC target genes and purine metabolism (Supplementary Fig. S2A). IS defining low-risk patients with DLBCL presented a significant enrichment in genes involved in immune response (Supplementary Fig. S2B). Altogether, these data highlight a deregulation of iron metabolism genes in association with a poor outcome in DLBCL (**Fig. 1F**). This argued in favor of iron homeostasis representing a potential therapeutic target for high-risk patients with DLBCL.

Targeting iron homeostasis kills DLBCL cells

According to these results, we investigated the therapeutic effect of well-established iron chelators including deferoxamine and deferasirox using two ABC cell lines OCI-LY3 and U-2932 and two GCB cell lines DB and SUDHL-5. A concentration-dependent reduction in cell viability following treatment with deferoxamine or deferasirox was identified. The IC_{50} values obtained with deferoxamine were 3.75, 3.24, 2.42, and 1.55 μmol/L against OCI-LY3, DB, U2932, and SUDHL5 cells, respectively (**Fig. 2A**). In comparison, the 50% IC_{50} values obtained for deferasirox were 9.50, 13.9, 4.79, and 1.48 μmol/L in OCI-LY3, DB, U2932, and SUDHL5 cells, respectively (**Fig. 2B**). In contrast, ironomycin induced a dose-dependent decrease in cell viability with nanomolar IC_{50} values compared with deferoxamine and deferasirox (16.8, 17.2, 30.4, and 28.9 nmol/L in OCI-LY3, DB, U2932, and SUDHL5 cells, respectively; **Fig. 2C**).

We extended these analyses to a panel of 16 DLBCL cell lines. For all these cell lines, ironomycin exhibited IC_{50} values within nanomolar range of concentrations (range: 7.2–91.5 nmol/L; Supplementary Fig. S3A and S3B). Using Affymetrix U133P gene expression profiling, the Iron score was calculated for 9 DLBCL cell lines. A significant correlation between the iron score and the response to ironomycin was identified (Supplementary Fig. S3C).

To validate the antilymphoma activity of ironomycin *in vivo*, the A20 syngeneic immunocompetent model of murine lymphoma was used. *In vitro*, ironomycin exhibited an IC_{50} of 200 nmol/L for the A20 cell line. Of note, this IC_{50} is 2.2 fold higher than the IC_{50} obtained for the most resistant human DLBCL cell line tested (Supplementary Fig. S3). Eight-week-old Balb/c mice were subcutaneously inoculated with A20 lymphoma cells and when the tumor was palpable the ironomycin treatment started (**Fig. 2D**). The tumor volume (mm^3) was assessed over time during the experiment. A significant difference in the tumor volume between vehicle-treated and ironomycin-treated (3 mg/kg i.p.) mice was identified (38% at day 27; $P < 0.05$; **Fig. 2D**). Of note, the total body weight of the mice was not affected by ironomycin treatment, suggesting that ironomycin is not toxic for the mice (Supplementary Fig. S3D).

Cancer cells frequently modulate intracellular iron homeostasis in ways that favor iron accumulation: toward increased iron uptake and storage, decreased iron export, or both. Interestingly, increased iron accumulation is also characteristic of tumor-initiating cells, cancer stem cells and mesenchymal cancer cells (11, 15, 16). Because the labile iron pool (LIP) is critical for tumor cell metabolism, we investigated the effect of ironomycin on LIP in DLBCL cells. LIP was measured by flow cytometry according the procedure of Prus and colleagues (17). Cells were loaded with 0.25 μmol/L Calcein-AM for 15 minutes, then washed and treated for 1 hour with deferasirox or ironomycin. Mean fluorescence intensity (MFI) of unstained cells and CA-stained cells treated with deferasirox or ironomycin was measured. Differences in MFI before and after treatment with deferasirox (ΔF) represent the amount of LIP. Interestingly, ironomycin treatment significantly decreased LIP in DLBCL cell lines (**Fig. 2E**) linked to the relocalization of iron in the lysosome mediated by ironomycin. Because ironomycin and iron chelators deplete LIP, we investigated the effect of iron supplementation on the cell death induced by these small molecules. The concentrations of iron-targeting small molecules were chosen according the maximal plasmatic concentration achievable in the patient (18, 19). Iron chelators and ironomycin induces apoptosis in OCI-LY3 and DB cell lines monitored by Annexin V and PARP cleavage (**Fig. 3A**). Iron supplementation significantly inhibited the effect of iron chelators on DLBCL cells apoptosis (**Fig. 3B**; $P < 0.05$ and $P < 0.01$ for deferoxamine and deferasirox treatment, respectively). However, iron supplementation did not affect ironomycin-induced DLBCL cell cytotoxicity illustrating distinct modes of action (**Fig. 3B**). We next sought to identify the mechanisms involved in ironomycin induced DLBCL cell death. Dose-dependent ironomycin-DLBCL-cell cytotoxicity was demonstrated using LDH release-assay (Supplementary Fig. S4A). Ironomycin treatment resulted in 7-AAD$^+$/Annexin V$^+$ and 7-AAD$^+$/Annexin V$^-$ death profiles in DLBCL cells as previously reported by Mai and colleagues in breast cancer (Supplementary Fig. S4B and S4C; ref. 11). Apoptosis induced by ironomycin in DLBCL cell lines was partially inhibited by the pan-caspase inhibitor Quinoline-Val-Asp-Difluorophenoxy-methylketone (Oph-Q-VD; $P < 0.001$; **Fig. 3C**) and was associated with activation of caspase-3, -7 and -9, which could be rescued by adding Oph-Q-VD (**Fig. 3D**). Ironomycin was shown to induce ferroptosis in breast mesenchymal cancer cells (11). Here, we found that ironomycin induced ferroptosis in DLBCL cells as monitored by Bodipy-C11 staining indicating the presence of lipid peroxidation, using erastin as positive control (Supplementary Figs. S5C and S6A). Consistently, ironomycin-induced cell death could be partially prevented by the ferroptosis inhibitor ferrostatin-1 (Supplementary Figs. S5A and S5B and S6B–S6D; ref. 12). We

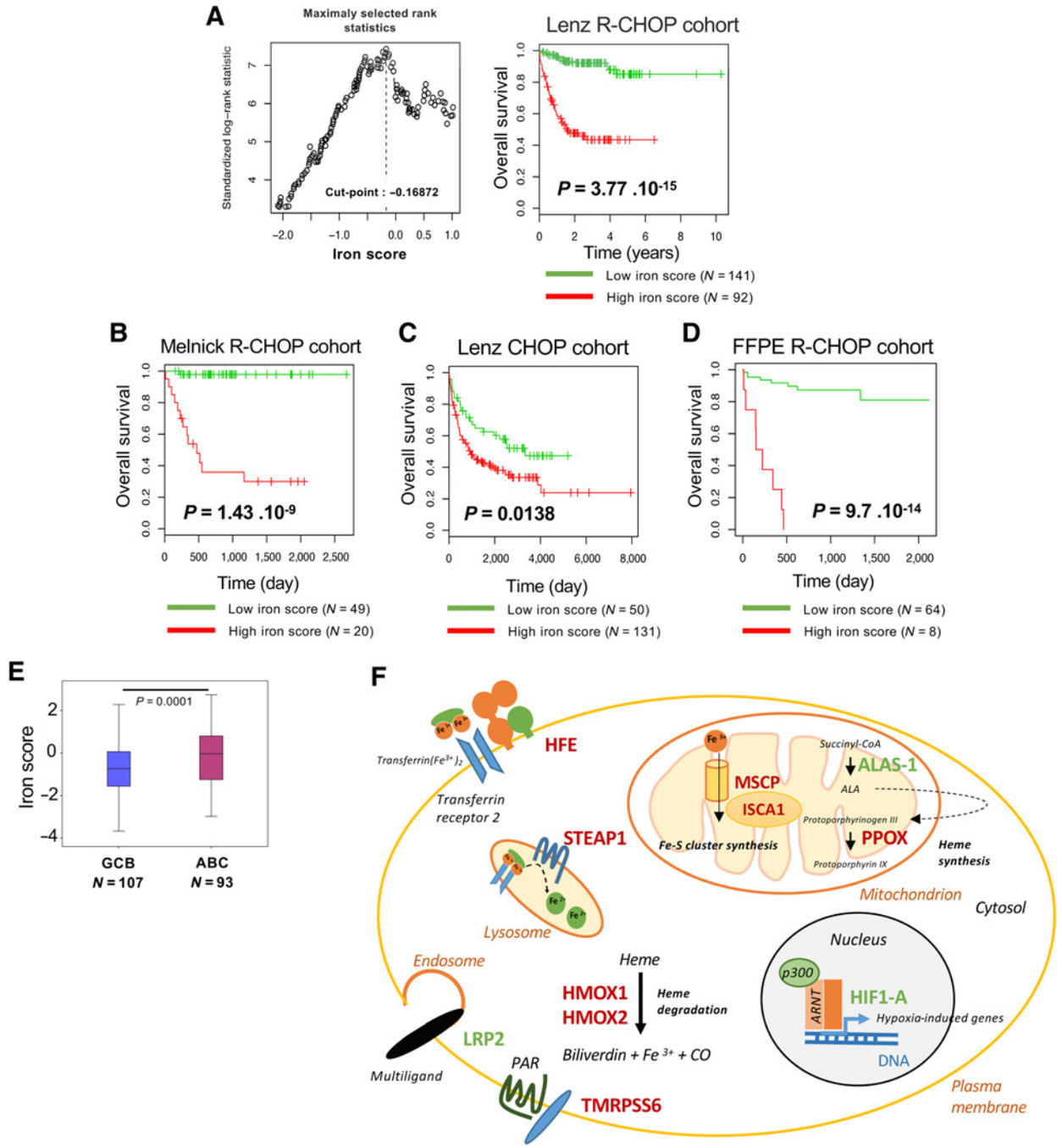

Figure 1.

Prognostic value of the iron score in patients with DLBCL. **A,** Patients of the Lenz R-CHOP cohort ($n = 233$) were ranked according to increased iron score, and a maximum difference in OS was obtained with iron score of -0.16872 splitting patients into high-risk and low-risk groups. **B–D,** Iron score also had a prognostic value in three other independent cohorts of patients (Melnick R-CHOP cohort, Lenz CHOP cohort, and FFPE R-CHOP cohort). **E,** Iron score is significantly higher in ABC compared with GCB DLBCL patients. **F,** Prognostic genes involved in iron homeostasis in DLBCL. Green, genes associated with a better outcome; red, genes associated with a poor outcome in patients with DLBCL.

also tested β-mercaptoethanol (B-ME) and liproxstatin as a ferroptosis inhibitor. B-ME rescued the toxicity induced by erastin, a ferroptosis inductor, but not the effects mediated by ironomycin in DLBCL cells (Supplementary Fig. S5D). Liproxstatin significantly inhibits the DLBCL cytotoxicity mediated by ironomycin and erastin treatment (Supplementary Fig. S5E). Ironomycin presents an antineoplastic effect by accumulating and sequestering iron in lysosomes, leading to cytoplasmic depletion of iron, degradation of ferritin in lysosomes

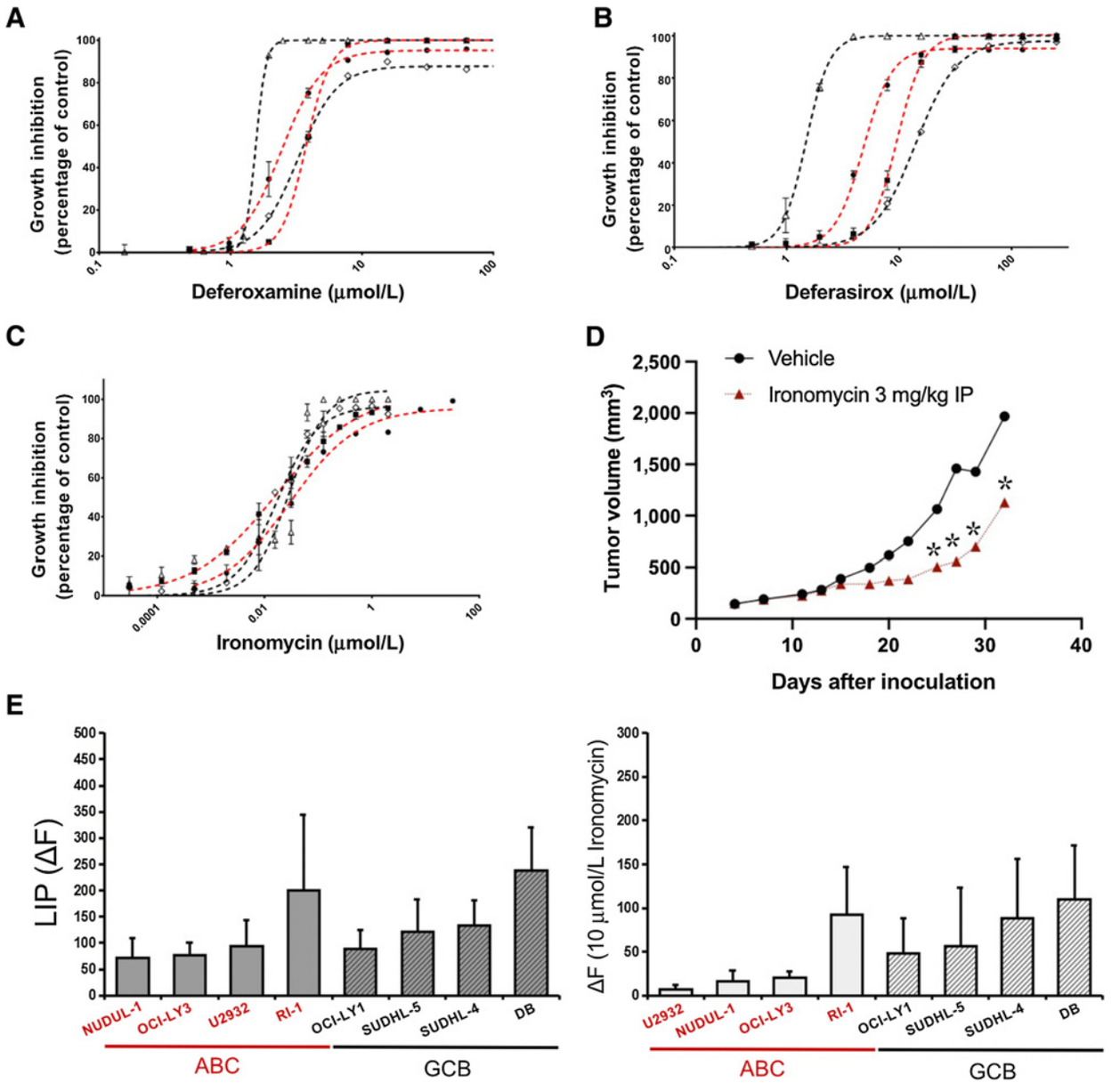

Figure 2.

Iron chelators and ironomycin inhibit DLBCL cell growth and decrease the LIP. **A–C,** DLBCL cells were incubated with different concentrations of iron chelators or vehicle for 96 hours. IC_{50} was calculated with concentration–response curve after treatment with deferoxamine (**A**), deferasirox (**B**), and ironomycin (**C**). **D,** Cell viability was examined using quantification of ATP assay. Data are expressed as mean percentage ± SEM of at least three independent experiments performed in six times. Balb/c mice were inoculated with murine A20 lymphoma cells and when tumor was palpable, the mice were treated with ironomycin (3 mg/kg i.p.). Mice were sacrificed when tumor volume reached 1,500 mm^3. Evaluation of the tumor volume of vehicle ($n = 10$) and ironomycin-treated mice ($n = 10$). *, $P < 0.05$ using Mann–Whitney test. **E,** Effect of Ironomycin on LIP was measured by dequenching of Calcein. Cells were loaded with 0.25 μmol/L Calcein-AM for 15 min, washed, and incubated for 1 hour with or without 100 μmol/L deferasirox or 10 μmol/L ironomycin. In this experiment, following treatment, cells were washed and their fluorescence was measured by flow cytometry. The difference in the mean fluorescence index between chelator-treated and untreated cells (ΔF) is presented. The results represent the mean and SD of at least four independent experiments.

and production of ROS activating ferroptosis cell death (20, 21). Because the ferroptosis inhibition of B-ME is mediated by promotion of cysteine uptake (22), this could explain the results obtained with ironomycin. Importantly, the identification of features of apoptosis and ferroptosis illustrate the heterogeneous nature of DLBCL cells susceptible to trigger different cell death pathways in distinct subpopulations. The expression of the autophagy-associated protein LC3I-II (23) was significantly increased in DLBCL cells following treatment with ironomycin (100 nmol/L, 24 hours). We identified a clear increase in LC3B-II puncta in DLBCL cells upon ironomycin treatment ($P < 0.0001$; Supplementary Fig. S7A and S7B). However, the ironomycin-induced autophagy was lower than BIX-01294, a G9a/GLP inhibitor used as positive control (24).

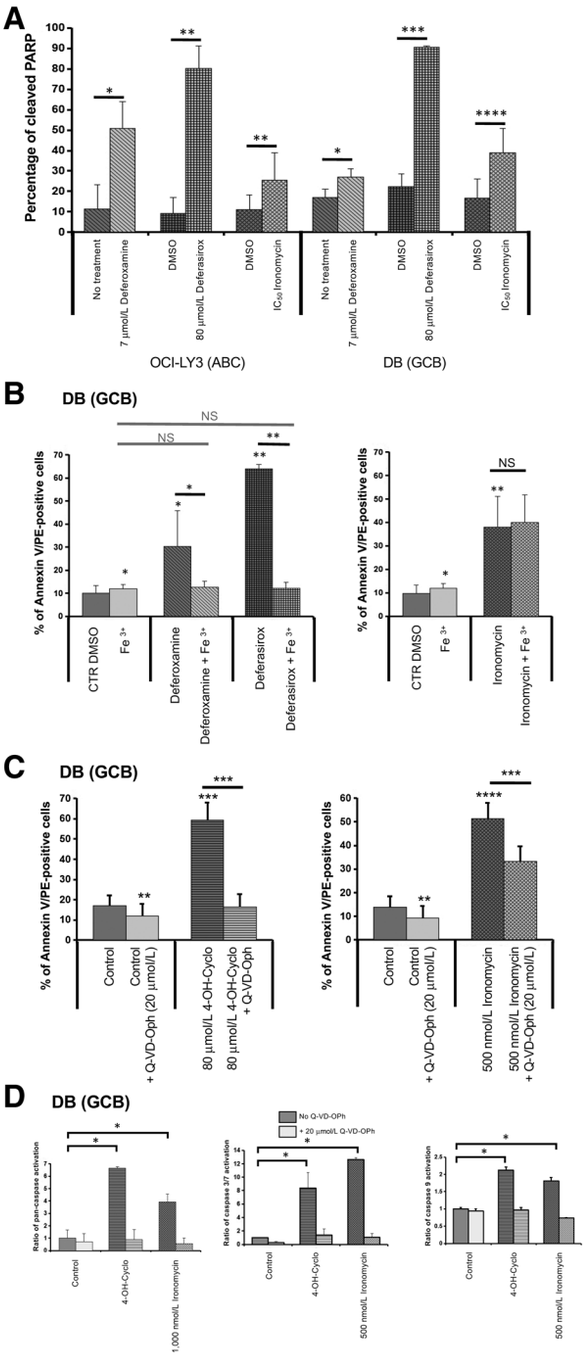

Figure 3.

Effect of ironomycin on apoptosis induction. **A,** Effect of deferoxamine (7 μmol/L), deferasirox (80 μmol/L), and ironomycin (IC_{50}) on PARP cleavage was analyzed using flow cytometry after 72 hours for OCI-LY3 and DB cells. Results represent the mean percentage and SEM of three independent experiments. **B,** DB cell line was preincubated with or without 7 μmol/L of deferoxamine, 80 μmol/L of deferasirox, or IC_{50} of ironomycin for 4 hours, followed by 72-hour incubation in presence or absence of $FeCl_3$ (100 μmol/L). Apoptosis was assessed using Annexin V-PE staining by flow cytometry. **C,** Cells were pretreated at least 30 minutes by 20 μmol/L of Q-VD-Oph as pan-caspase inhibitor before treatment. DB cells were treated as indicated during 48 hours; effect of ironomycin on apoptosis was analyzed using Annexin V/PE staining by flow cytometry. 4-OH-cyclophosphamide (80 μmol/L) was used as a positive control. **D,** Results represent the mean ± SD of Annexin V–positive cells of three independent experiments. DB cell line was treated as indicated during 24 hours, and pan-caspase, caspase-3/7, and caspase-9 activities were measured by luminescence. 4-OH-cyclophosphamide (80 μmol/L) was used as a positive control. Results are mean ± SD of three experiments. Statistical significance was tested using paired Student *t* test: *, $P < 0.05$; **, $P < 0.01$; ***, $P < 0.001$; ****, $P < 0.0001$; NS, nonsignificant.

These data underline that ironomycin perturbs autophagic flux in DLBCL cells. Because ferritinophagy may be involved in the observed ironomycin-mediated autophagy (11), we investigated ferritin degradation after ironomycin treatment. Ironomycin treatment resulted in significant ferritin degradation in DLBCL cells supporting ferritinophagy induction (Supplementary Fig. S7C).

Iron can catalyze the production of ROS through Fenton chemistry. Treatment of OCI-LY3 and DB DLBCL cells with iron chelators or ironomycin induces ROS production monitored by fluorescein probe 5-(and-6)-chloromethyl-2′,7′-dichlorodihydrofluorescein diacetate-acetyl ester (CM-H2DCFDA) staining (**Fig. 4A** and **B**). ROS production mediated by ironomycin was partially inhibited by ferrostatin (**Fig. 4C**; Supplementary Fig. S8A). Chaetocin was used as positive control (25). Scavenging ROS with DFO significantly reduced the percentage of ROS-positive cells and ROS levels in ironomycin-treated cells (**Fig. 4C**). DFO partly prevented ironomycin from killing DLBCL cells. Ascorbate did not demonstrated significant effects (Supplementary Fig. S8B). However, only low dose of ascorbate was reported to inhibit ferroptosis induction whereas moderate to high doses of ascorbate have no significant effect. Ironomycin treatment resulted in a significant decrease of the GSH/GSSG ration without significant GSH depletion (Supplementary Fig. S8C). Taken together, these results are consistent with the hypothesis that ironomycin kills DLBCL cells to some extent through the production of reactive oxygen species.

Ironomycin affects DLBCL cell division and induces a DNA damage response

To investigate the effects of iron depletion on the proliferation of DLBCL cells, OCI-LY3 and DB cell lines were treated with iron chelators and ironomycin and cell-cycle distribution was assessed 72 hours after treatment. The iron chelator deferasirox and ironomycin significantly affected cell-cycle distribution of surviving cells with a blockade of BrdU incorporation and an increase in the G_0–G_1 phase (**Fig. 5A** and **B**). Moreover, Western blot and immunofluorescence analyses revealed that all drugs increased the phosphorylation of the histone H2AX variant (γH2AX) levels in OCI-LY3 and DB cells (**Fig. 5C** and **D**), which is indicative of DNA damage.

To characterize the origin of the chromosome breaks induced by ironomycin, we next monitored the impact of this drug on DNA replication. Indeed, eukaryotic cells contain numerous iron-sulfur (Fe-S) cluster proteins that play key roles in DNA replication and require iron as a cofactor (4). To investigate whether ironomycin promotes DNA breaks by increasing replication stress, we next used the DNA fiber spreading technique to monitor fork progression in DLBCL cells treated with ironomycin. When cells were treated with ironomycin during the CldU pulse, we observed a reduction of fork speed in both cell lines (4.5-fold for DB and 3.7-fold for OCI-LY3), indicating that ironomycin strongly inhibits DNA synthesis ($P < 0.0001$; **Fig. 6A** and **B**). Remarkably, the effect of ironomycin was even stronger than the inhibition mediated by gemcitabine.

Gemcitabine impedes DNA synthesis by inhibiting the production of dNTPs by RNR (26, 27). Because iron is essential for RNR

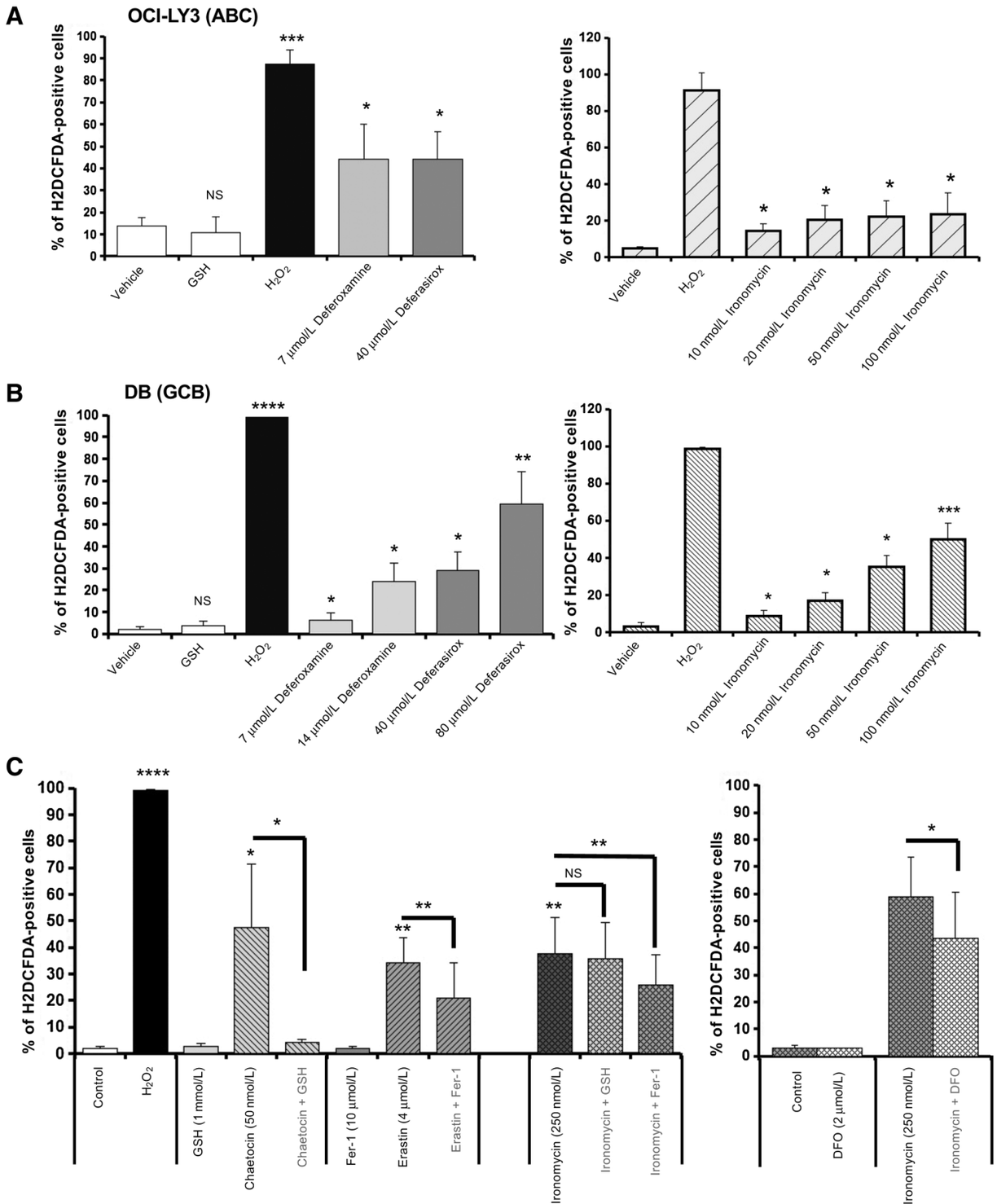

Figure 4.

Iron chelators and ironomycin induce ROS production in DLBCL cells. **A** and **B,** Effect of deferoxamine, deferasirox, and ironomycin on the ROS production was analyzed using flow cytometry after oxidation of a CM-H2DFDA probe for OCI-LY3 (**A**) and DB cell line (**B**) at 48 hours. **C,** Vehicle and GSH treatment (5 and 0.5 mmol/L, respectively, 1 hour) was used as a negative control and oxygen peroxide (10 mmol/L, 1 hour) as a positive control. For the ROS reversion assay, DB cells were treated with 250 nmol/L Ironomycin for 48 hours with or without GSH or Fer-1 or deferoxamine (DFO). ROS production was analyzed using flow cytometry after oxidation of a CM-H2DFDA probe. Chaetocin and erastin were used as positive control for GSH and Fer-1 reversion, respectively. Results represent the mean percentage and SD of three independent experiments. *, $P < 0.05$; **, $P < 0.01$; ***, $P < 0.001$; ****, $P < 0.0001$; NS, nonsignificant; with paired Student t test.

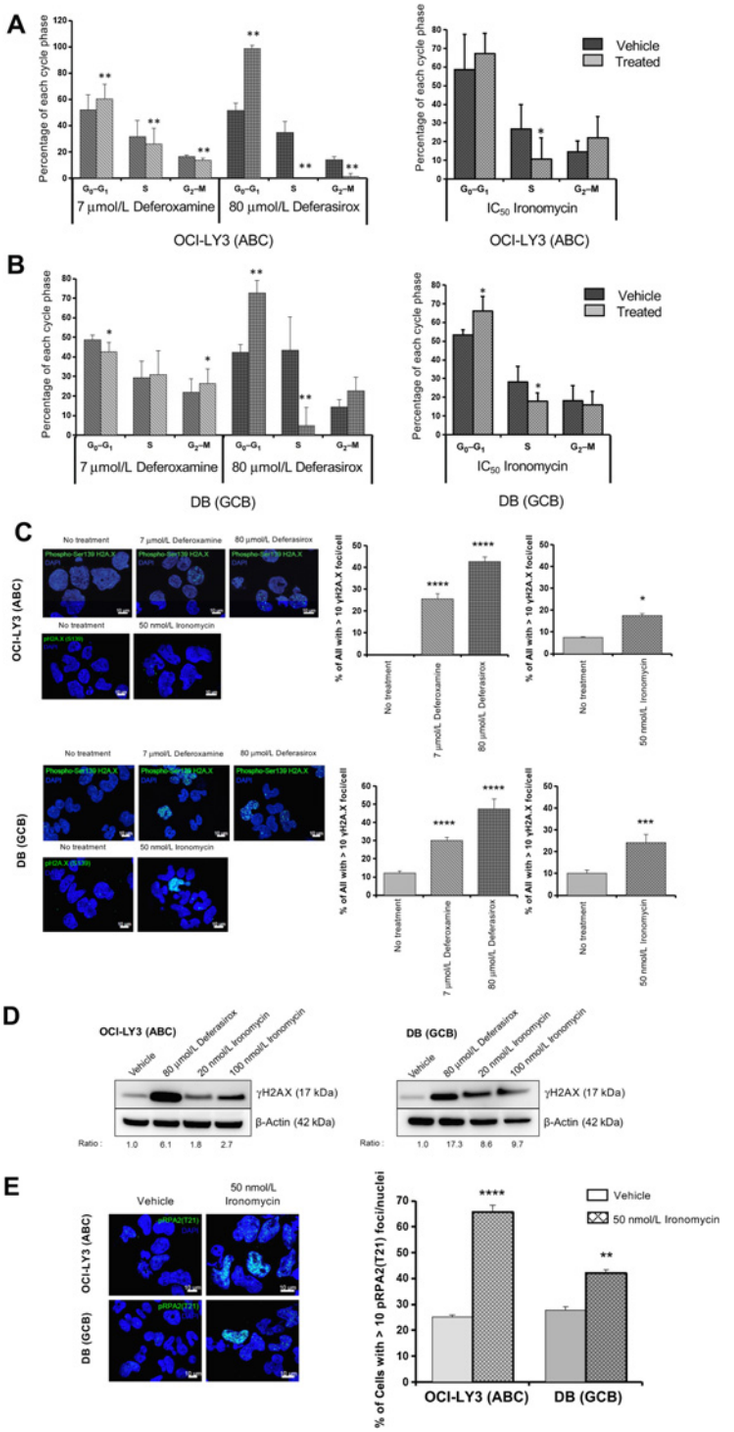

Figure 5.

Ironomycin induced G_1–S cell-cycle arrest and DNA damage. **A** and **B,** Cells were incubated with vehicle, with 7 μmol/L deferoxamine, 80 μmol/L deferasirox, or with IC_{50} ironomycin for 72 hours. Cell cycle was analyzed using flow cytometry, S phase was stained by an anti-BrdU antibody after BrdU incorporation, and DNA content was strained by 4′,6-diamidino-2-phénylindole (DAPI) for OCI-LY3 (**A**) and DB cells (**B**). Histograms represent the mean percentage and SEM of each cell-cycle phase of three independent experiments. *, $P < 0.05$; **, $P < 0.01$, with paired Student *t* test. **C,** Cells were incubated with vehicle or with 7 μmol/L deferoxamine, 80 μmol/L deferasirox, or 50 nmol/L ironomycin for 24 hours. Double-strand break induction was monitored by γH2AX staining and nuclei were stained with DAPI. Foci were visualized by fluorescence microscopy. Original magnification, ×63. Scale bar, 10 μm. The percentage of cells with more than 10 γH2AX foci per cell (± SEM) is displayed in the histograms. **D,** Cells were treated with iron chelators (80 μmol/L deferasirox) and ironomycin (20 and 100 nmol/L) during 24 hours. Protein levels of γH2AX were analyzed by Western blot. **E,** DB and OCI-LY3 cells were treated with 50 nmol/L ironomycin during 24 hours. Immunofluorescence staining for foci of phospho-RPA2 T21 and DAPI was performed (magnification, ×63). Scale bar, 10 μm. The percentage of cells with more than 10 phospho-RPA2 T21 foci per cell is displayed in the histograms. At least 300 cells were counted for each group. Statistical difference was tested using a Fisher's exact test. *, $P < 0.05$, **, $P < 0.01$, ***, $P < 0.001$, ****, $P < 0.0001$. NS, nonsignificant.

activity (3, 28), we next asked whether ironomycin also acts on dNTP pools to inhibit DNA replication. To this end, we complemented cells with exogenous nucleosides (+ dN) 30 minutes before the addition of Ironomycin and Gemcitabine (**Fig. 6C**). DNA fiber spreading revealed that IdU tracks were significantly shorter in the presence of dN compared with nonsupplemented cells (**Fig. 6D**), indicating that exogenous nucleosides slow down DNA synthesis in DLBCL cells, presumably by altering the balance of intracellular dNTP pools. In contrast, dN increased the speed of replication forks by two-fold in the presence of gemcitabine (**Fig. 6D**), which is consistent with the fact that this drug inhibits DNA synthesis by depleting dNTP pools. Interestingly, dN also increased fork speed in cells exposed to Ironomycin, but to a lower extent (1.25 fold) than in cells exposed to gemcitabine (**Fig. 6D**). This suggests that unlike

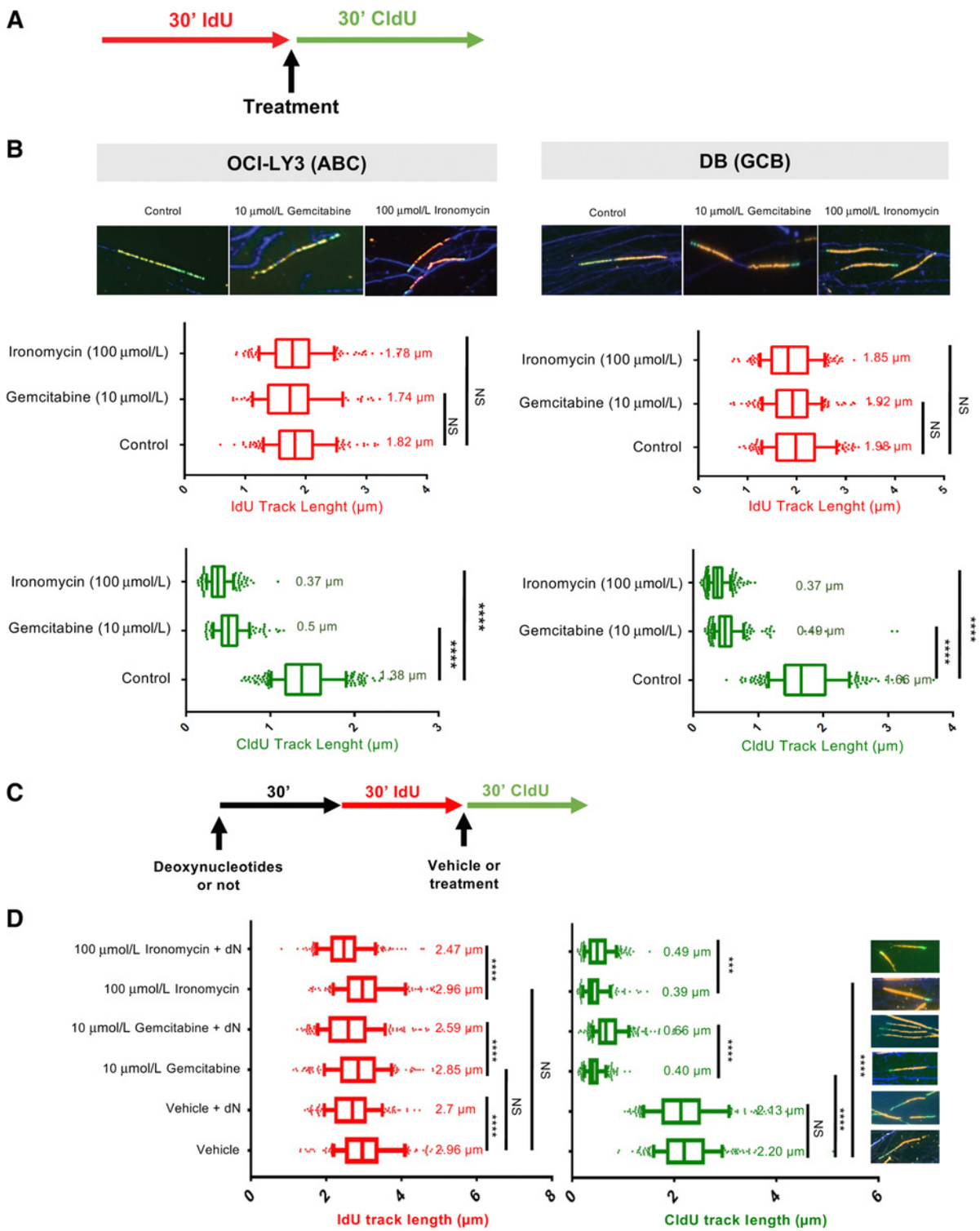

Figure 6.

Ironomycin induces defective DNA replication fork progression. **A** and **B,** DB and OCI-LY3 cells were labeled with IdU, treated with vehicle, gemcitabine (10 µmol/L) or ironomycin (100 µmol/L) and labeled with CldU (30 minutes each), and then harvested for DNA fiber assay. **C** and **D,** DB cells were pretreated or not by deoxynucleotides for 30 minutes, labeled with IdU, treated with vehicle, gemcitabine (10 µmol/L) or ironomycin (100 µmol/L) and labeled with CldU (30 minutes each), and then harvested for DNA fiber assay. Boxplot represents median ± interquartile ranges and dots represent outliers of track length (expressed in µm). Results represent at least 200 track measurements. ***, $P < 0.001$; ****, $P < 0.0001$; NS, nonsignificant, Mann–Whitney test.

gemcitabine, ironomycin targets other DNA replication enzymes, in addition to RNR. Altogether, these data indicate that ironomycin impedes cell-cycle progression by inducing a massive slowdown of replication forks and this replication stress activates the ATR kinase, as illustrated by the phosphorylation of RPA32 on T21 (**Fig. 5E**). MYC deregulation, through different mechanisms, could be detected in 40% of patients with DLBCL in association with a poor outcome (29, 30). Interestingly, iron chelator and ironomycin treatment induced a significant downregulation of c-MYC oncogene expression at RNA and protein levels (Supplementary Fig. S9A and S9B). Analyzing 16 DLBCL cell lines, no significant correlation between the basal c-MYC level and the response to ironomycin was found (Supplementary Fig. S9C).

Iron depletion induces cell death of primary DLBCL cells and sensitizes cells to doxorubicin, BCL2, BTK, and Syk kinase inhibitors

To further support the fact that iron depletion represents an attractive therapeutic strategy in DLBCL, primary samples of patients with DLBCL were cultured with their microenvironment recombinant CD40 L in presence of 50 and 100 nmol/L ironomycin. Ironomycin treatment significantly reduced the median number of viable primary DLBCL cells by 63.1% ($P = 0.02$, $N = 5$) and 67.1% ($P = 0.006$, $N = 5$) at 50 and 100 nmol/L, respectively (**Fig. 7A**; Supplementary Fig. S10A and S10B). Interestingly, ironomycin demonstrated a higher toxicity in DLBCL cells compared with normal cells from the microenvironment (**Fig. 7B** and **C**). We investigated the level of intracellular iron in DLBCL samples using RhoNox-1 probe. Of interest, DLBCL cells of patients demonstrate a significant higher level of intracellular iron compared with normal cells from the microenvironment (**Fig. 7D**; Supplementary Fig. S10C) supporting the observed high sensitivity of DLBCL cells to ironomycin. Ironomycin treatment resulted in PI^+/Annexin V^+ and PI^+/Annexin V^- death profiles in DLBCL primary cells as previously reported by Mai and colleagues in breast cancer (**Fig. 8A**; Supplementary Fig. S10D; ref. 11). Furthermore, ironomycin significantly increases membrane transferrin receptor 1 (TFR1; CD71) expression, a specific marker of ferroptosis (**Fig. 8B**; ref. 31).

We then investigated the effect of ironomycin combined with conventional drugs commonly used in DLBCL (e.g., doxorubicin, etoposide, cyclophosphamide). Cells were treated with increasing concentrations of ironomycin and increasing concentration of conventional chemotherapy agents. Synergy matrix was built applying the Bliss equation from the viability matrix (32). Ironomycin significantly potentiated the toxicity of doxorubicin in DLBCL cells (**Fig. 7E**). A lower additive effect combining 4-OH-cyclophosphamide or etoposide with ironomycin was also identified (Supplementary Fig. S11A–S11C). These data were validated using primary samples from patients (**Fig. 7B**). Combination of ironomycin with doxorubicin demonstrated a significantly higher toxicity compared with monotherapy ($P < 0.05$, $N = 5$) with a reduction of viable DLBCL cells of 92.3% (**Fig. 7B**). We also tested the synergy between ironomycin and targeted therapies including BCL2 inhibitor, BTK inhibitor and Syk kinase inhibitor. Ironomycin significantly potentiates the effect of BCL2 inhibitor venetoclax in ABC DLBCL cell lines (Supplementary Fig. S12A). Ironomycin treatment resulted in BCL2, MCL1, and BCLXL protein expression decrease. The protein expression reduction of antiapoptotic proteins after ironomycin treatment could support the observed synergy. According to these results, we investigated the combination of ironomycin with MCL1 inhibitor (AZD-5991) and BCL-XL inhibitor (A1155463). Interestingly, ironomycin synergizes with AZD-5991 and A1155463 to induce DLBCL cell toxicity (Supplementary Fig. S12B–S12D).

A synergy between ironomycin and BTK inhibitor ibrutinib or Syk kinase inhibitor entospletinib was also identified (Supplementary Fig. S13A and S13B). To investigate the ironomycin-associated hematopoietic toxicity, hematopoietic progenitor colony-forming unit (CFU) assays were performed with $CD34^+$ cells from apheresis of five normal donors. Cells were cultured in hydroxyl-methyl-cellulose medium with conventional chemotherapy (5 μmol/L of 4-OH-cyclophosphamide or 200 nmol/L doxorubicin) or ironomycin (10, 50, or 100 nmol/L). Cyclophosphamide and doxorubicin induced a major toxicity of 81.8% and 99% of mean growing progenitors compared with the control. Ironomycin treatment exhibited no significant toxicity when used at 10 nmol/L on CFU-C, CFU-E, and CFU-GM formation ($N = 5$). Treatment with 50 and 100 nmol/L of ironomycin demonstrated a significant lower hematopoietic toxicity compared with conventional chemotherapy (**Fig. 7D**).

Altogether, these data demonstrate that a subgroup of high-risk patients with DLBCL identified by the IS could benefit from targeting of iron homeostasis using ironomycin alone or in combination with doxorubicin, BCL2, BTK or Syk kinase inhibitors.

Discussion

Here, we identified that deregulation of iron homeostasis gene expression is associated with a prognostic value in independent cohorts of patients with DLBCL, allowing the creation of an iron-based gene expression risk score (IS). IS represents an independent prognostic factor when compared with GCB or ABC subtype, age, and IPI. IS is enriched in genes involved in iron uptake, iron utilization, storage and export. Among them, STEAP1 ferrireductase was reported to be associated with a poor outcome in several cancers (33). STEAP1 does not possess metalloreductase activity, but colocalizes with the TF-TFR1 complex in endosomes, underlining a role in iron metabolism. STEAP1 is a driver of cancer invasion, proliferation and immune escape (34). Heme-oxygenase 1 (HMOX1) overexpression is associated with a higher risk of relapse in patients with acute myeloid leukemia (35). The activity of heme-oxygenase 1 was shown to promote metastasis of breast cancer cells through increase of intracellular iron level, migration and invasion (36). Tumor cells from patients with DLBCL with high-risk IS are associated with a significant enrichment in MYC target genes and purine metabolism. Interestingly, key c-MYC-target genes are transferrin receptor 1 (TFR1) and divalent metal ion transporter 1 (DMT1) that increase intracellular LIP linking oncogenic signaling and iron metabolism (37). Interestingly, iron chelator and ironomycin treatment induced a significant downregulation of c-MYC oncogene expression at RNA and protein levels (Supplementary Fig. S9) together with TFR1 downregulation. High level of c-MYC protein expression is associated with a poor outcome in DLBCL (38). More recently, high *TFRC* expression was also shown to be associated with a poor outcome in patients with DLBCL (39). Ironomycin treatment may represent an interesting therapeutic strategy in aggressive patients with DLBCL characterized by MYC overexpression even if no significant correlation between c-MYC protein expression and response to ironomycin was identified.

Recent analyses underlined that intracellular pH modification by Fenton reaction may play a major role in tumorigenesis and cancer development (40). Depleting intracellular iron stores represents attractive therapeutic opportunities in cancer (41). Here, we demonstrated that ironomycin, a synthetic derivate of salinomycin (11) known to sequester iron in the lysosome and to induce cancer stem cell death

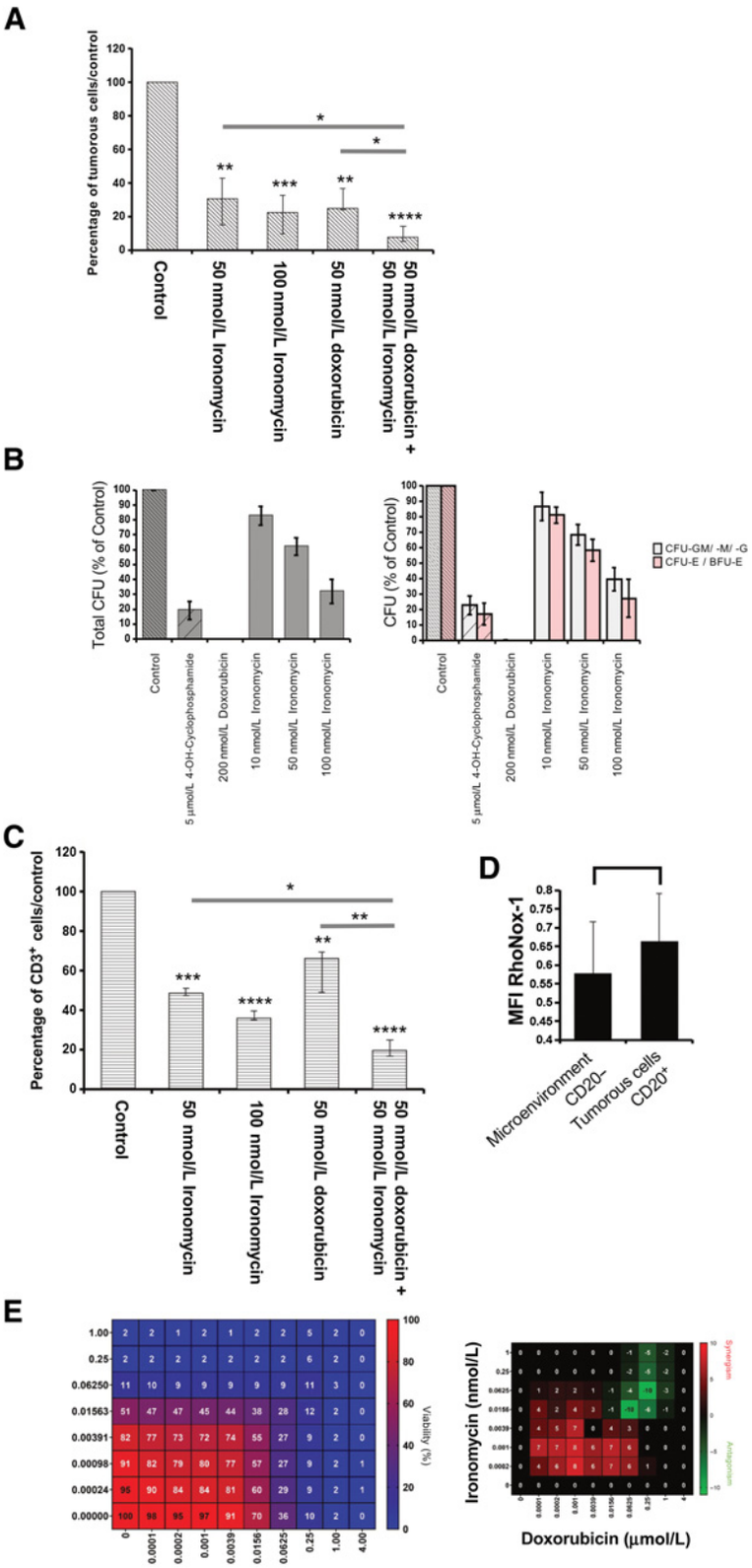

Figure 7.

Ironomycin presents a significant toxicity on DLBCL primary cells and potentializes doxorubicin cytotoxicity. **A,** Primary DLBCL cells were treated with ironomycin and/or doxorubicin and incubated during 96 hours with CD40L. DLBCL cell toxicity was analyzed by flow cytometry. **B,** Hematopoietic progenitor CFU assay were performed with $CD34^+$ cells from apheresis of 5 donors. Cells were cultured in hydroxyl-methyl-cellulose medium with or without conventional chemotherapy or ironomycin. CFU-C, CFU-E, and CFU-GM were counted after 14-day culture. **C,** The toxicity of ironomycin alone or in combination with doxorubicin on normal $CD3^+$ cells was assessed by flow cytometry. Results represent the median ± interquartile ranges of each population ($n = 5$ patients). Statistical significance was tested using t test of pairs: *, $P < 0.05$; **, $P < 0.01$; ***, $P < 0.001$; ****, $P < 0.0001$. **D,** Primary DLBCL cells of 6 patients and PBMC of a healthy donor were incubated with 5 µmol/L Rho-Nox1 Fe^{2+} probe. The MFI was assessed by flow cytometry in $CD20^+$ DLBCL cells and $CD20^-$ cells (microenvironment cells). **E,** DB cells were treated with increasing concentrations of ironomycin combined with doxorubicin for 96 hours, and cell viability was tested by ATP quantification to obtain the viability matrix. The synergy matrix was calculated as described in Materials and Methods.

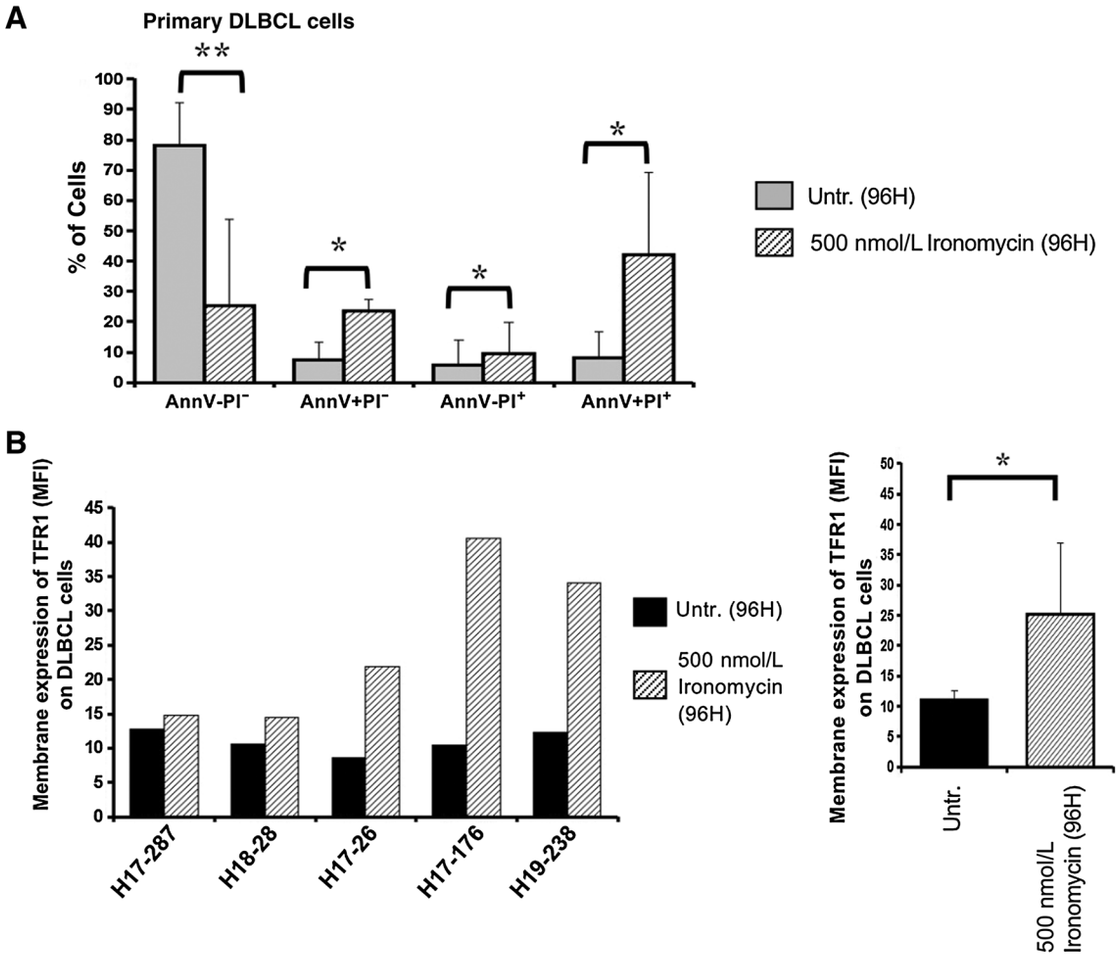

Figure 8.

Ironomycin induces mortality and TFR1 downregulation in primary DLBCL cells. **A,** Primary DLBCL cells from four patients were cultured with recombinant CD40 L in the presence or absence of ironomycin (500 nmol/L). After 96 hours, cell death of DLBCL cells was monitored by Annexin V/PI staining using flow cytometry. Results represent the mean ± SD. **B,** Primary samples of patients with DLBCL were cultured with recombinant CD40 L in presence or absence ironomycin (500 nmol/L). DLBCL cell membrane TFR1 (CD71) expression was assessed by flow cytometry. *, $P < 0.05$; **, $P < 0.01$.

induces major toxicity at nanomolar concentration in all the DLBCL cell lines tested, independently of the cell of origin status. Compared with iron chelators, the toxicity mediated by ironomycin could not be reversed by iron supplementation. This difference between the activity of iron chelators and ironomycin is interesting because it was also demonstrated that iron chelators decrease mitochondrial iron-dependent lipid peroxidation and ferroptosis preventing heart damage in cardiomyopathy models (42, 43). Ironomycin induced significant cell growth inhibition, apoptosis, ferroptosis and perturb autophagic flux in DLBCL cells. Of major interest, ironomycin demonstrated a more selective toxicity on primary DLBCL cells compared with normal cells from the microenvironment. Furthermore, previous data demonstrated the favorable toxicity profile of ironomycin in mice without generic toxicity. Ironomycin reduced tumor growth of breast cancer patient–derived xenografts without detectable toxicity at effective doses (11). However, deeper investigations of ironomycin toxicity with a particular focus on potential liver damage should be developed for future clinical applications. We also observed a low toxicity of ironomycin on human hematopoietic progenitors with modest effect on CFU-C, CFU-E, and CFU-GM colony formation compared with conventional chemotherapy. Due to significantly higher proliferation and DNA synthesis rates, cancer cells require more iron compared with normal cells. Iron is indispensable in maintaining the activity of iron- or heme-containing enzymes including enzymes involved in DNA replication and repair, Jumonji (JmjC) domain-containing histone demethylases involved in epigenetic modification and mitochondrial oxidases involved in respiratory complexes (8, 44).

Our data also indicate that ironomycin interferes with the progression of DLBCL cells through the cell cycle. To decipher the molecular mechanism involved, we have monitored the effect of this drug on DNA replication. Remarkably, DNA fiber studies revealed that ironomycin treatment is associated with replication forks slowing, comparable to the effect of the RNR inhibitor gemcitabine. The RNR complex requires iron to convert rNTPs in dNTPs and is therefore essential for DNA replication (45). Interestingly, exogenous nucleosides increased replication fork speed in cells treated with gemcitabine or ironomycin, which is consistent with the idea that these drugs target RNR. However, this rescue was less pronounced for ironomycin than for gemcitabine, suggesting that besides RNR, ironomycin inhibits other iron-dependent enzymes involved in DNA replication and repair.

Ironomycin also increased the phosphorylation of H2AX and of the ATR-specific target RPA32 (T21), indicating that it provokes a replication stress in DLBCL cells. These data underlined that impairment of cell-cycle progression is a major mechanism of perturbing iron homeostasis in DLBCL. Furthermore, ironomycin synergized with doxorubicin to kill DLBCL cell lines and primary DLBCL cells from patients. Together, these data indicate that ironomycin targets key enzymes involved in DNA replication and repair and represents therefore a promising molecule for DLBCL treatment. Furthermore, a significant synergy was identified when ironomycin is combined with BH3 mimetics, BTK or Syk kinase inhibitors that are currently in clinical development in DLBCL. Of interest, ironomycin treatment resulted in BCL2, MCL1 and BCLXL protein expression downregulation that could support the observed synergy between ironomycin and BH3 mimetics in DLBCL cells. Furthermore, double-expressor DLBCL (DE-DLBCL), defined by the overexpression of MYC and BCL2 proteins, and double-hit DLBCL, defined as a dual translocation of *MYC* together with *BCL2* define subgroups of high-risk DLBCL with poor outcome (46). This could be due to the cell proliferation deregulation by c-MYC, without apoptosis induction in the presence of BCL2 overexpression. BCL2 inhibitors are currently in clinical trials in DLBCL. The addition of BCL2 inhibitor to R-CHOP recently demonstrated the potential to improve the outcome of patients with BCL2 overexpressed DLBCL (47). Combination of BCL2 inhibitor and ironomycin may be of clinical interest in this aggressive subgroup of patients. The synergy between ironomycin and BTK or Syk kinase inhibitors may be related to cholesterol metabolism. Cholesterol plays an important role in BCR signaling (48). After ligand binding, BCRs cluster and rapidly associate with lipid rafts (49, 50). SYK is recruited to BCR clusters associated with lipid rafts and protein tyrosine phosphorylation is enhanced in these regions (50). SYK and BTK regulate cholesterol biosynthesis and associated integrity of BCR in lipid rafts (48, 51). Rink and colleagues reported that inhibition of cholesterol uptake reduces GPX4 expression and induces ferroptosis (52). We identified a significant downregulation of GPX4 protein level after treatment with ironomycin in DLBCL cells. GPX4 possesses a unique capability to detoxify hydroperoxides in complex lipids, even when they are into lipoproteins or membranes, protecting membranes from peroxidation damage. The role of SYK and BTK (48, 51) in the regulation of cholesterol biosynthesis together with the GPX4 downregulation mediated by ironomycin could support the synergy identified when ironomycin is combined with BTK and SYK inhibitors. Furthermore, we investigated the therapeutic interest to combine ironomycin, an inhibitor of cholesterol biosynthesis (ketoconazole) and BTK or SYK inhibitors. Of Interest, addition of ketoconazole to ironomycin/BTK or SYK inhibitors induces a higher toxicity on DLBCL cells (Supplementary Fig. S14A–S14D).

Iron could also play a role in transcriptional regulation of cancer cells mediated epigenetic reprogramming. Iron dependent modifications of histone or DNA methylation have been shown to play a significant role in solid cancers (53, 54). Previous studies have demonstrated the high frequency of somatic mutations in genes that encode epigenetic enzymes in B-cell lymphomas (55). In this context, targeting iron homeostasis may induce significant epigenetic changes modifying expression of key genes involved in DLBCL tumorigenesis and progression.

Approximately 30% to 40% of patients will develop relapsed or refractory disease that remains a major cause of morbidity and mortality. Further improvements in therapy and novel therapeutic strategies are urgently needed for these patients with relapsed/refractory and high-risk biological subtypes of DLBCL. More rational therapies are therefore needed both for high-risk patients in the up-front setting and for those with relapse/refractory-DLBCL. In addition, even those currently cured up-front or, especially, after salvage therapy and stem-cell transplant for relapse/refractory DLBCL face long-term toxicities including secondary malignancies. Our data demonstrate that targeting iron homeostasis using ironomycin could be of therapeutic interest, especially in high-risk DLBCL defined by the IS and in relapsed/refractory patients where current treatment remains ineffective until the recent evidence emerging from chimeric antigen receptor T-cell therapy.

Authors' Disclosures

J. Devin reports a patent for WO-2021089819-A1:Iron-score and *in vitro* method for identifying high-risk DLBCL subjects and therapeutic uses and methods licensed. T. Cañeque reports a patent for PCT-EP2020081349 issued. G. Cartron reports personal fees from Roche, BMS-Celgene, Abbvie, Takeda, MedxCell, MabQi, Jansen, Gilead, and Novartis outside the submitted work. R. Rodriguez reports grants from Fondation Charles-Defforey and Ligue Nationale Contre le Cancer during the conduct of the study; in addition, R. Rodriguez has a patent for PCT-EP2020081349 issued and a patent for WO2016038223 issued; and is a founder of SideROS. J. Moreaux reports grants from INCA (Institut national du Cancer)/French government, French National Agency for Research (ANR), and Carnot Institute of Lymphoma (ICALYM) during the conduct of the study; in addition, J. Moreaux has a patent for Iron-score and *in vitro* method for identifying high-risk DLBCL subjects and therapeutic uses and methods (EP2020081349) issued. No disclosures were reported by the other authors.

Authors' Contributions

J. Devin: Conceptualization, data curation, formal analysis, investigation, writing–original draft. **T. Cañeque:** Data curation, formal analysis, investigation, writing–review and editing. **Y.-L. Lin:** Data curation, supervision, investigation, methodology, writing–review and editing. **L. Mondoulet:** Investigation, writing–review and editing. **J.-L. Veyrune:** Investigation, writing–review and editing. **M. Abouladze:** Resources, investigation. **E. Garcia De Paco:** Resources, investigation. **O. Karmous Gadacha:** Resources, investigation. **G. Cartron:** Conceptualization, data curation, writing–review and editing. **P. Pasero:** Conceptualization, data curation, writing–review and editing. **C. Bret:** Conceptualization, data curation, supervision, validation, methodology, writing–original draft, project administration, writing–review and editing. **R. Rodriguez:** Conceptualization, data curation, supervision, funding acquisition, validation, methodology, writing–original draft, project administration, writing–review and editing. **J. Moreaux:** Conceptualization, supervision, funding acquisition, validation, methodology, writing–original draft, project administration, writing–review and editing.

Acknowledgments

The authors thank the imaging facility MRI, member of the national infrastructure France-Bioimaging supported by the French National Research Agency (ANR-10-INBS-04, Investments for the future). The R. Rodriguez research group is funded by the European Research Council (ERC) under the European Union's Horizon 2020 research and innovation program (grant agreement no. 647973) and the Fondation Charles Defforey-Institut de France and Ligue Contre le Cancer (Equipe Labellisée). The authors also thank the CNRS, INSERM, and Institut Curie for generous funding. The J. Moreaux research group was supported by grants from INCA PLBIO18-362 PIT-MM and PLBIO19 FATidique, ANR (TIE-Skip; 2017-CE15-0024-01), ANR-18-CE15-0010-01 PLASMADIFF-3D, SIRIC Montpellier Cancer (INCa_Inserm_D-GOS_12553), Carnot FINDMED, Institut Carnot CALYM, Labex EpiGenMed, and Institut Universitaire de France. Work in the P. Pasero lab is supported by grants from the Agence Nationale pour la Recherche (ANR), INCA, the Ligue Nationale Contre le Cancer (équipe labellisée), and the Fondation MSDAvenir.

The costs of publication of this article were defrayed in part by the payment of page charges. This article must therefore be hereby marked *advertisement* in accordance with 18 U.S.C. Section 1734 solely to indicate this fact.

Received January 20, 2021; revised August 14, 2021; accepted January 21, 2022; published first January 25, 2022.

References

1. Reddy A, Zhang J, Davis NS, Moffitt AB, Love CL, Waldrop A, et al. Genetic and functional drivers of diffuse large B cell lymphoma. Cell 2017;171:481–94.
2. Staudt LM, Dave S. The biology of human lymphoid malignancies revealed by gene expression profiling. Adv Immunol 2005;87:163–208.
3. Torti SV, Torti FM. Iron and cancer: More ore to be mined. Nat Rev Cancer 2013; 13:342–55.
4. Zhang C. Essential functions of iron-requiring proteins in DNA replication, repair and cell cycle control. Protein Cell 2014;5:750–60.
5. Wu Y, Brosh RM Jr. DNA helicase and helicase-nuclease enzymes with a conserved iron-sulfur cluster. Nucleic Acids Res 2012;40:4247–60.
6. Le NT, Richardson DR. The role of iron in cell cycle progression and the proliferation of neoplastic cells. Biochim Biophys Acta 2002;1603:31–46.
7. Muller S, Sindikubwabo F, Caneque T, Lafon A, Versini A, Lombard B, et al. CD44 regulates epigenetic plasticity by mediating iron endocytosis. Nat Chem 2020;12:929–38.
8. Yu Y, Kovacevic Z, Richardson DR. Tuning cell cycle regulation with an iron key. Cell Cycle 2007;6:1982–94.
9. Vazana-Barad L, Granot G, Mor-Tzuntz R, Levi I, Dreyling M, Nathan I, et al. Mechanism of the antitumoral activity of deferasirox, an iron chelation agent, on mantle cell lymphoma. Leuk Lymphoma 2013;54:851–9.
10. Pullarkat V, Meng Z, Donohue C, Yamamoto VN, Tomassetti S, Bhatia R, et al. Iron chelators induce autophagic cell death in multiple myeloma cells. Leuk Res 2014;38:988–96.
11. Mai TT, Hamai A, Hienzsch A, Caneque T, Muller S, Wicinski J, et al. Salinomycin kills cancer stem cells by sequestering iron in lysosomes. Nat Chem 2017;9:1025–33.
12. Dixon SJ, Lemberg KM, Lamprecht MR, Skouta R, Zaitsev EM, Gleason CE, et al. Ferroptosis: An iron-dependent form of nonapoptotic cell death. Cell 2012;149: 1060–72.
13. Miller LD, Coffman LG, Chou JW, Black MA, Bergh J, D'Agostino R Jr, et al. An iron regulatory gene signature predicts outcome in breast cancer. Cancer Res 2011;71:6728–37.
14. Herviou L, Kassambara A, Boireau S, Robert N, Requirand G, Muller-Tidow C, et al. PRC2 targeting is a therapeutic strategy for EZ score defined high-risk multiple myeloma patients and overcome resistance to IMiDs. Clin Epigenetics 2018;10:121.
15. Basuli D, Tesfay L, Deng Z, Paul B, Yamamoto Y, Ning G, et al. Iron addiction: A novel therapeutic target in ovarian cancer. Oncogene 2017;36:4089–99.
16. Schonberg DL, Miller TE, Wu Q, Flavahan WA, Das NK, Hale JS, et al. Preferential iron trafficking characterizes glioblastoma stem-like cells. Cancer Cell 2015;28:441–55.
17. Prus E, Fibach E. Flow cytometry measurement of the labile iron pool in human hematopoietic cells. Cytometry A 2008;73:22–7.
18. Porter JB. Deferoxamine pharmacokinetics. Semin Hematol 2001;38:63–8.
19. Nisbet-Brown E, Olivieri NF, Giardina PJ, Grady RW, Neufeld EJ, Sechaud R, et al. Effectiveness and safety of ICL670 in iron-loaded patients with thalassaemia: A randomised, double-blind, placebo-controlled, dose-escalation trial. Lancet 2003;361:1597–602.
20. Hou W, Xie Y, Song X, Sun X, Lotze MT, Zeh HJ 3rd, et al. Autophagy promotes ferroptosis by degradation of ferritin. Autophagy 2016;12:1425–8.
21. Mancias JD, Wang X, Gygi SP, Harper JW, Kimmelman AC. Quantitative proteomics identifies NCOA4 as the cargo receptor mediating ferritinophagy. Nature 2014;509:105–9.
22. Ishii T, Bannai S, Sugita Y. Mechanism of growth stimulation of L1210 cells by 2-mercaptoethanol in vitro. Role of the mixed disulfide of 2-mercaptoethanol and cysteine. J Biol Chem 1981;256:12387–92.
23. Orhon I, Reggiori F. Assays to monitor autophagy progression in cell cultures. Cells 2017;6:20.
24. Ding J, Li T, Wang X, Zhao E, Choi JH, Yang L, et al. The histone H3 methyltransferase G9A epigenetically activates the serine-glycine synthesis pathway to sustain cancer cell survival and proliferation. Cell Metab 2013;18: 896–907.
25. Isham CR, Tibodeau JD, Jin W, Xu R, Timm MM, Bible KC. Chaetocin: A promising new antimyeloma agent with in vitro and in vivo activity mediated via imposition of oxidative stress. Blood 2007;109:2579–88.
26. Baker CH, Banzon J, Bollinger JM, Stubbe J, Samano V, Robins MJ, et al. 2′-Deoxy-2′-methylenecytidine and 2′-deoxy-2′,2′-difluorocytidine 5′-diphosphates: Potent mechanism-based inhibitors of ribonucleotide reductase. J Med Chem 1991;34:1879–84.
27. Heinemann V, Xu YZ, Chubb S, Sen A, Hertel LW, Grindey GB, et al. Inhibition of ribonucleotide reduction in CCRF-CEM cells by 2′,2′-difluorodeoxycytidine. Mol Pharmacol 1990;38:567–72.
28. Eklund H, Uhlin U, Farnegardh M, Logan DT, Nordlund P. Structure and function of the radical enzyme ribonucleotide reductase. Prog Biophys Mol Biol 2001;77:177–268.
29. Valera A, Lopez-Guillermo A, Cardesa-Salzmann T, Climent F, Gonzalez-Barca E, Mercadal S, et al. MYC protein expression and genetic alterations have prognostic impact in patients with diffuse large B-cell lymphoma treated with immunochemotherapy. Haematologica 2013;98:1554–62.
30. Kramer MH, Hermans J, Wijburg E, Philippo K, Geelen E, van Krieken JH, et al. Clinical relevance of BCL2, BCL6, and MYC rearrangements in diffuse large B-cell lymphoma. Blood 1998;92:3152–62.
31. Feng H, Schorpp K, Jin J, Yozwiak CE, Hoffstrom BG, Decker AM, et al. Transferrin receptor is a specific ferroptosis marker. Cell Rep 2020;30:3411–23.
32. Combes E, Andrade AF, Tosi D, Michaud HA, Coquel F, Garambois V, et al. Inhibition of Ataxia-telangiectasia mutated and RAD3-related (ATR) overcomes oxaliplatin resistance and promotes antitumor immunity in colorectal cancer. Cancer Res 2019;79:2933–46.
33. Moreaux J, Kassambara A, Hose D, Klein B. STEAP1 is overexpressed in cancers: A promising therapeutic target. Biochem Biophys Res Commun 2012;429:148–55.
34. Gomes IM, Maia CJ, Santos CR. STEAP proteins: From structure to applications in cancer therapy. Mol Cancer Res 2012;10:573–87.
35. Lu Y, Wu D, Wang J, Li Y, Ma D, Chai X, et al. Identification of heme oxygenase-1 as a novel predictor of hematopoietic stem cell transplantation outcomes in acute leukemia. Cell Physiol Biochem 2016;39:1495–502.
36. Kim DH, Kim JH, Kim EH, Na HK, Cha YN, Chung JH, et al. 15-Deoxy-Delta12,14-prostaglandin J2 upregulates the expression of heme oxygenase-1 and subsequently matrix metalloproteinase-1 in human breast cancer cells: Possible roles of iron and ROS. Carcinogenesis 2009;30:645–54.
37. O'Donnell KA, Yu D, Zeller KI, Kim JW, Racke F, Thomas-Tikhonenko A, et al. Activation of transferrin receptor 1 by c-Myc enhances cellular proliferation and tumorigenesis. Mol Cell Biol 2006;26:2373–86.
38. Kluk MJ, Chapuy B, Sinha P, Roy A, Dal Cin P, Neuberg DS, et al. Immunohistochemical detection of MYC-driven diffuse large B-cell lymphomas. PLoS One 2012;7:e33813.
39. Arumov A, Liyanage PY, Trabolsi A, Roberts ER, Li L, Ferreira B, et al. Optimized doxorubicin chemotherapy for diffuse large B-cell lymphoma exploits nanocarrier delivery to transferrin receptors. Cancer Res 2021;81:763–75.
40. Sun H, Zhang C, Cao S, Sheng T, Dong N, Xu Y. Fenton reactions drive nucleotide and ATP syntheses in cancer. J Mol Cell Biol 2018;10:448–59.
41. Brown RAM, Richardson KL, Kabir TD, Trinder D, Ganss R, Leedman PJ. Altered iron metabolism and impact in cancer biology, metastasis, and immunology. Front Oncol 2020;10:476.
42. Fang X, Wang H, Han D, Xie E, Yang X, Wei J, et al. Ferroptosis as a target for protection against cardiomyopathy. Proc Natl Acad Sci U S A 2019;116:2672–80.
43. Tang D, Chen X, Kang R, Kroemer G. Ferroptosis: molecular mechanisms and health implications. Cell Res 2021;31:107–25.
44. Wang Y, Yu L, Ding J, Chen Y. Iron metabolism in cancer. Int J Mol Sci 2018;20:95.
45. Puig S, Ramos-Alonso L, Romero AM, Martinez-Pastor MT. The elemental role of iron in DNA synthesis and repair. Metallomics 2017;9:1483–500.
46. Sesques P, Johnson NA. Approach to the diagnosis and treatment of high-grade B-cell lymphomas with MYC and BCL2 and/or BCL6 rearrangements. Blood 2017;129:280–8.
47. Morschhauser F, Feugier P, Flinn IW, Gasiorowski R, Greil R, Illes A, et al. A phase 2 study of venetoclax plus R-CHOP as first-line treatment for patients with diffuse large B-cell lymphoma. Blood 2021;137:600–9.
48. Chen L, Monti S, Juszczynski P, Ouyang J, Chapuy B, Neuberg D, et al. SYK inhibition modulates distinct PI3K/AKT- dependent survival pathways and cholesterol biosynthesis in diffuse large B cell lymphomas. Cancer Cell 2013;23: 826–38.
49. Dykstra M, Cherukuri A, Sohn HW, Tzeng SJ, Pierce SK. Location is everything: Lipid rafts and immune cell signaling. Annu Rev Immunol 2003;21:457–81.
50. Gupta N, DeFranco AL. Lipid rafts and B cell signaling. Semin Cell Dev Biol 2007; 18:616–26.
51. Rink JS, Yang S, Cen O, Taxter T, McMahon KM, Misener S, et al. Rational targeting of cellular cholesterol in diffuse large B-cell lymphoma (DLBCL) enabled by functional lipoprotein nanoparticles: A therapeutic strategy dependent on cell of origin. Mol Pharm 2017;14:4042–51.

52. Rink JS, Lin AY, McMahon KM, Calvert AE, Yang S, Taxter T, et al. Targeted reduction of cholesterol uptake in cholesterol-addicted lymphoma cells blocks turnover of oxidized lipids to cause ferroptosis. J Biol Chem 2021;296:100100.
53. Tsai YP, Chen HF, Chen SY, Cheng WC, Wang HW, Shen ZJ, et al. TET1 regulates hypoxia-induced epithelial-mesenchymal transition by acting as a co-activator. Genome Biol 2014;15:513.
54. Yamamoto S, Wu Z, Russnes HG, Takagi S, Peluffo G, Vaske C, et al. JARID1B is a luminal lineage-driving oncogene in breast cancer. Cancer Cell 2014;25:762–77.
55. Sermer D, Pasqualucci L, Wendel HG, Melnick A, Younes A. Emerging epigenetic-modulating therapies in lymphoma. Nat Rev Clin Oncol 2019;16:494–507.